

High-order accurate hybrid LES/PDF simulation of a supersonic coaxial lifted jet flame

Harshad D. Ranadive¹, Bruno Savard^{1,2}, Evatt R. Hawkes¹

¹University of New South Wales, Sydney, New South Wales, Australia

²University of Ottawa, Ottawa, Ontario, Canada

1 Introduction

In many modern engines, combustion occurs in the presence of high speed turbulent flows, for example in afterburners of aircraft engines or scramjet engines [1]. Typically in such flows, the flow time scales are small enough to overlap with the chemical time scales resulting in finite rate chemistry effects. Such turbulence-chemistry interactions (TCI) are also coupled with shocks and expansion waves in the flow field. Conducting laboratory experiments of such configurations is challenging and hence the development of numerical solvers is vital for the better understanding of flame dynamics.

Large-eddy simulations (LES) are a class of numerical simulations in which the large scales of turbulence are explicitly resolved by the mesh while the sub-grid effects, that include the chemical reactions, are modelled. Transported probability density function (PDF) is a widely employed model for turbulent combustion [2] in which the transport equations for the sub-grid joint PDF's of the state variables (typically species mass fraction and enthalpy) are solved. As a result, the nonlinear chemical source term appears in closed form in the PDF formulation. The PDF model has been studied extensively with low Mach solver formulations; however, a limited number of studies have attempted to employ this model within fully compressible implementations [3].

Hybrid solvers are typically used for LES/PDF simulations in which an Eulerian solver provides the resolved velocity field, turbulent diffusivity and pressure to a Lagrangian solver which in turn updates a stochastic particle system that mimics the evolution of the joint PDF's. Most of the PDF solvers [3,4] employ the first-order accurate Euler–Maruyama scheme for time integration of the particle stochastic differential equations (SDE's) and spatially first-order accurate particle-in-cell (PIC) scheme [5] for the estimation of particle means. Wang et al. [6] presented second-order accurate temporal integration schemes for the SDE's in a low Mach solver formulation. Such implementations have not been noted in compressible LES/PDF solvers.

The current solver features second-order accurate temporal integration for the SDE's (in a weak¹ sense) along with spatially second-order accurate particle algorithms for mean estimation and interpolation [5]. The above implementation is an extension to the Fortran-based compressible solver S3D [7], developed originally for direct numerical simulations. In the current work, the extended LES/PDF solver is applied to an experimental supersonic H₂/air lifted flame that was studied by Cheng et al. [8].

¹Weak convergence implies for the statistics as opposed to strong convergence that implies for the trajectories

2 Methodology

The filtered fully compressible system of equations solved on an Eulerian mesh are given below:

$$\frac{\partial \bar{\rho}}{\partial t} = -\nabla \cdot (\bar{\rho} \tilde{\mathbf{u}}), \quad (1)$$

$$\frac{\partial \bar{\rho} \tilde{\mathbf{u}}}{\partial t} = -\nabla \cdot [\bar{\rho} \tilde{\mathbf{u}} \tilde{\mathbf{u}} + \bar{p} \tilde{\boldsymbol{\delta}} - \tilde{\boldsymbol{\tau}}], \quad (2)$$

$$\frac{\partial \bar{\rho} \tilde{E}}{\partial t} = -\nabla \cdot \left[(\bar{\rho} \tilde{E} + \bar{p}) \tilde{\mathbf{u}} + \mathbf{q} - \tilde{\boldsymbol{\tau}} \cdot \tilde{\mathbf{u}} \right], \quad (3)$$

$$\frac{\partial \bar{\rho} \tilde{Y}_\alpha}{\partial t} = -\nabla \cdot [\bar{\rho} \tilde{\mathbf{u}} \tilde{Y}_\alpha + \mathbf{J}_\alpha] + \tilde{\omega}_\alpha + \tilde{F}_\alpha, \quad (4)$$

where the over-bar ($\bar{\phi}$) denotes a filtered variable and the tilde ($\tilde{\phi}$) denotes a Favre filtered variable ($\overline{\rho\phi}/\bar{\rho}$), ρ is the density, p is the pressure, \mathbf{u} is the velocity, $\boldsymbol{\delta}$ is the unit tensor, $\boldsymbol{\tau}$ is the viscous and SGS stress tensor, \mathbf{q} is the molecular and SGS heat flux vector and $\tilde{E} = \tilde{\mathbf{u}} \cdot \tilde{\mathbf{u}}/2 + \tilde{h} - \bar{p}/\bar{\rho}$ is the specific total energy (comprised of internal (e) and kinetic energy) with h denoting the gas enthalpy. For each species denoted by $\alpha = 1, 2, \dots, N_s$ (N_s is the total number of species), Y_α is its mass fraction, \mathbf{J}_α is its molecular and SGS diffusive flux and ω_α is its chemical source term (determined from the Lagrangian solver). Mixture-averaged transport properties are utilised to evaluate the molecular viscosity, conductivity and species mass diffusivity. The ideal gas assumption is used for the equation of state. The term \tilde{F}_α applies a relaxation feedback from the Lagrangian solver to the Eulerian solver using the mean particle compositions ($\langle Y_\alpha \rangle$) [9] in order to enforce consistency on the redundant Eulerian composition variables. The timescale of the feedback is much larger than the simulation time step.

The SGS stress tensor is evaluated using the artificial shear viscosity model while the SGS heat flux vector is evaluated using the artificial thermal conductivity model as discussed by Cook [10]. The turbulent species diffusivities are evaluated from the artificial thermal conductivity based on the assumption of unity turbulent Lewis number.

In the PDF model, the transport equation for the sub-grid joint PDF's of the composition variables (species mass fraction and internal energy) is solved using an equivalent Lagrangian system given as [3]

$$d\mathbf{x}^* = \left[\tilde{\mathbf{u}} + \frac{\nabla(\bar{\rho}\Gamma_{\text{SGS}})}{\bar{\rho}} \right]^* dt + \sqrt{2\Gamma_{\text{SGS}}^*} d\mathbf{W}^*, \quad (5)$$

$$de^* = -\Omega_m (h^* - \langle h \rangle^*) dt + \left[\frac{1}{\bar{\rho}} \nabla \cdot \mathbf{q}^{\text{m}} \right]^* dt + \left[\frac{1}{\bar{\rho}} (\tilde{\boldsymbol{\tau}} : \nabla \tilde{\mathbf{u}} - \bar{p} \nabla \cdot \tilde{\mathbf{u}}) \right]^* dt, \quad (6)$$

$$dY_\alpha^* = -\Omega_m (Y_\alpha^* - \langle Y_\alpha \rangle^*) dt + \left[\frac{1}{\bar{\rho}} \nabla \cdot \mathbf{J}_\alpha^{\text{m}} \right]^* dt + \left[\frac{1}{\bar{\rho}} \right]^* \dot{\omega}_\alpha^* dt, \quad (7)$$

where the superscript ϕ^* denotes a quantity (ϕ) at the particle position, $\langle \cdot \rangle$ denotes the Favre mean (estimated on the Eulerian grid), \mathbf{W} is a Wiener process, Γ_{SGS} is the turbulent diffusivity and \mathbf{q}^{m} and $\mathbf{J}_\alpha^{\text{m}}$ are the molecular heat flux and species mass diffusion flux respectively. Molecular mixing is modelled using the IEM model [11] and the mixing frequency (Ω_m) is evaluated using $\Omega_m = C_\phi (\Gamma + \Gamma_{\text{SGS}}) / \Delta^2$ [12], where Δ is the grid spacing, Γ is the molecular diffusivity and C_ϕ is the mechanical-to-scalar mixing time scale ratio taken as 2 [13].

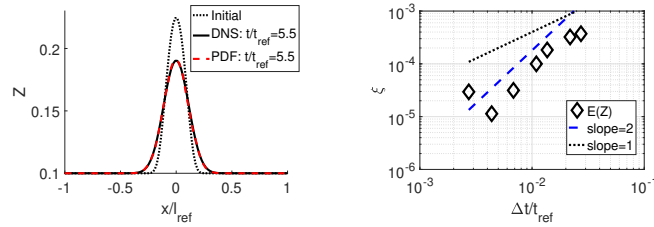


Figure 1: Left: initial and final profile for mixture fraction (Z); right: error ($\xi = \frac{|E(Z) - E(Z)_{ref}|}{E(Z)_{ref}}$) for different time step sizes where $E(\cdot)$ denotes the mathematical expectation

An explicit six-stage Runge-Kutta (RK) algorithm that is fourth-order accurate for the deterministic equations [14] and weak second-order accurate for the stochastic equations [15] is employed to integrate the governing equations in a tightly coupled manner. The spatial derivatives are evaluated using an eighth-order accurate central difference scheme, with a cubic skew-symmetric treatment of the convective terms [16]. An eighth-order Padé-type tridiagonal filter [17] is applied after regular intervals (10 time steps) to suppress the high-frequency numerical errors. Interpolation and mean estimation are done using the second-order accurate cloud-in-cell and linear spline (CIC/LS) approach as discussed in Viswanathan et al. [5]. Finally, particle number control algorithms are employed in order to maintain the particle count inside a finite difference cell within user specified bounds.

The temporal convergence of the solver is demonstrated with the aid of a 1D configuration involving turbulent mixing. A domain of length $L/l_{ref} = 8.8$ is sub-divided into 480 mesh points and initialised with a profile for mixture fraction (Z) as shown in Fig. 1 (left). The reference length scale is $l_{ref} = 8.74$ mm and the reference velocity scale $u_{ref} = 477$ m/s. The reference time scale is $t_{ref} = l_{ref}/u_{ref}$. The composition of the gas phase includes N_2 and O_2 , with $Z = 1$ in pure N_2 . Turbulent diffusivity is imposed artificially so that it is 100 times the magnitude of the local thermal diffusivity. Each Eulerian cell is initialised with 500 particles. The reference solution is obtained by using a small time step size of $\Delta t/t_{ref} = 5.5 \times 10^{-4}$ (and otherwise the same settings). The error in $E(Z)$ (where $E(\cdot)$ denotes the expectation computed using 100 independent simulations) at the domain mid-point and time $t/t_{ref} = 5.5$ is shown in Fig. 1 (right). The temporal error clearly shows a second-order convergence for the coupled LES/PDF solver.

3 Simulation Details

In the experiments by Cheng et al. [8], a fuel jet composed of hydrogen and a coaxial stream of burnt products are released into open atmosphere at fully expanded conditions. The specifications of the two streams and the ambient are summarised in Table 1.

Table 1: Experimental specifications of the supersonic lifted jet flame

| Stream | Diameter (mm) | Mach number | Temperature (K) | Pressure (kPa) | Reynolds number | Species mole fractions |
|---------|---------------|-------------|-----------------|----------------|-----------------|------------------------------------|
| Jet | 2.36 | 1 | 545 | 112 | 15,600 | $H_2=1.0$ |
| Co-flow | 17.78 | 2 | 1250 | 107 | 101,100 | $O_2=0.201, H_2O=0.255, N_2=0.544$ |
| Ambient | | 0 | 300 | 101 | 0 | $O_2=0.21, N_2=0.79$ |

A cuboidal computational domain of size $70D$ in the axial direction and $50D$ in the transverse directions is used, where D is the jet diameter. The mesh has a uniform resolution of $280 \mu\text{m}$ in the region lying within a distance of $\pm 8D$ from the jet centreline while it is stretched in the far-field regions. Assuming a model spectrum for the turbulent kinetic energy (slope $= -5/3$) and using the integral length scales available from the experiment, approximately 90% of the turbulent kinetic energy is resolved by this mesh. A small time step size of 2×10^{-8} seconds (acoustic CFL number of 0.12) is utilised. A chemical mechanism involving 9 species and 21 reactions was obtained by reducing the detailed Aramcomech 3.0 mechanism [18].

The domain is initialised uniformly along the axis with experimental data at $x/D = 0.85$. Turbulent fluctuations to the axial velocity at the inlet are provided using an isotropic turbulence feed generated using the Passot-Pouquet spectrum, and shaped to the profile of the jet. For the LES/PDF simulation, the particles are initialised with a random distribution on the Eulerian mesh and the initial composition variables are interpolated from the Eulerian data. The initial particle count in a cell (N_{pc}) is set to 30 and is bounded by $\{10, 60\}$ in the subsequent time steps.

4 Results and Discussion

The instantaneous contours of OH mole fraction superimposed on isolines of pressure and the temperature contours are shown in Fig. 2. The pressure isolines have 10 levels in the range from 0.5 to 1.5 atm and show significant spatial gradients as expected in such high-speed compressible flows. The contours of OH radical and temperature show that the flame primarily ignites after 20 jet diameters behind a weak pressure wave. The experiments reported that the lift-off length for this flame was approximately $x/D = 25$. Thus the simulation shows a slightly earlier ignition as compared to that reported in the experiment. These differences might be because the nozzle geometry was not modelled and the profiles of turbulent velocities at the inlet were not available from the experiments.

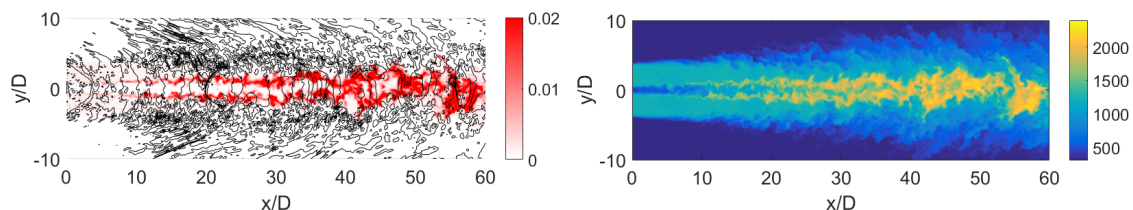


Figure 2: Left: instantaneous contours of OH mole fraction superimposed on pressure isolines between 0.5-1.5 atm with 10 levels; right: instantaneous contours of temperature for the supersonic lifted jet flame

Comparisons of mean and RMS axial velocity, temperature and mole fractions of H_2 , H_2O and OH at four axial stations are shown in Fig. 3. Axial velocity statistics are evaluated from the Eulerian solver, and are well predicted across the four stations. The statistics of temperature and species mole fractions are computed from the particle data. The predictions of temperature compare well with the experiment overall, with some differences at the farthest axial station ($x/D = 43.1$). The prediction of H_2 and H_2O also compare well for the first two stations. At $x/D = 32.3$ and $x/D = 43.1$ the results show that the flame has lower level of ignition near the jet centreline as compared to the experiment. Consistent with this observation the minor radical species OH is under-predicted at these farther stations. The RMS plots show that the fluctuations in temperature and species mole fractions are very high in the flow field which is a common feature of such high speed flows [8].

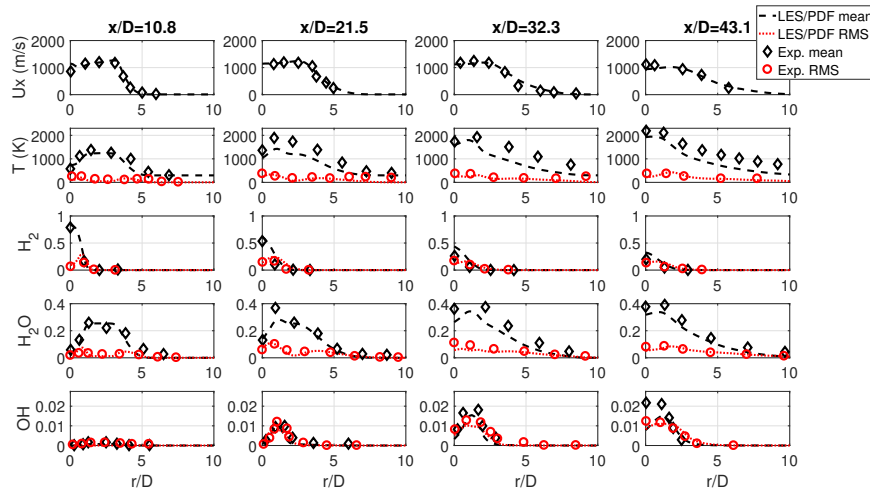


Figure 3: Comparison of statistics of axial velocity, temperature and species mole fractions at four axial stations for the supersonic lifted jet flame

5 Conclusion

An experimental supersonic lifted flame was simulated using a high-order accurate LES/PDF solver. Good predictions were shown for the statistics of axial velocity, temperature, major and minor species at different axial stations with the exception of the flame being under-predicted near the jet centreline at the downstream stations. Overall the results showed the capability of the LES/PDF solver to predict this challenging high speed turbulent flame. In future, the methodology can be applied to simulations of compressible turbulent reacting flows in practical configurations like gas turbine or scramjet engines.

6 Acknowledgements

This work was performed with funding support from the Australian Government Research Training Program Scholarship and the Australian Research Council (ARC). ARC support was provided via the Discovery Projects funding scheme (DP180103923, DP150104393), and via the Linkage Infrastructure, Equipment and Facilities scheme (LE170100032, LE160100002). The computational facilities supporting this project included the Australian National Computational Infrastructure (NCI) National Facility (the partner share of the NCI National Facility provided by Intersect Australia Pvt. Ltd.) and the Pawsey Supercomputing Centre (with funding support from the Australian Govt. and the Govt. of Western Australia).

References

- [1] E. D. Gonzalez-Juez, A. R. Kerstein, R. Ranjan, and S. Menon, "Advances and challenges in modeling high-speed turbulent combustion in propulsion systems," *Prog. Energy Combust. Sci.*, vol. 60, pp. 26–67, 2017.
- [2] D. C. Haworth, "Progress in probability density function methods for turbulent reacting flows," *Prog. Energy Combust. Sci.*, vol. 36, no. 2, pp. 168–259, 2010.

- [3] A. Banaeizadeh, Z. Li, and F. A. Jaber, "Compressible scalar filtered mass density function model for high-speed turbulent flows," *AIAA Journal*, vol. 49, no. 10, pp. 2130–2143, 2011.
- [4] V. Raman and H. Pitsch, "A consistent LES/filtered-density function formulation for the simulation of turbulent flames with detailed chemistry," *Proc. Combust. Inst.*, vol. 31, pp. 1711–1719, 2007.
- [5] S. Viswanathan, H. Wang, and S. B. Pope, "Numerical implementation of mixing and molecular transport in LES/PDF of turbulent reacting flows," *J. Comput. Phys.*, vol. 230, pp. 6916–6957, 2011.
- [6] H. Wang, P. P. Popov, and S. B. Pope, "Weak second-order splitting schemes for Lagrangian Monte Carlo particle methods for the composition PDF/FDF transport equations," *J. Comput. Phys.*, vol. 229, no. 5, pp. 1852–1878, 2010.
- [7] J. H. Chen, A. Choudhary, B. De Supinski, M. DeVries, E. R. Hawkes, S. Klasky, W. K. Liao, K. L. Ma, J. Mellor-Crummey, N. Podhorszki, R. Sankaran, S. Shende, and C. S. Yoo, "Terascale direct numerical simulations of turbulent combustion using S3D," *Comput. Sci. Discov.*, vol. 2, 2009.
- [8] T. S. Cheng, J. A. Wehrmeyer, R. W. Pitz, O. J. Jarret, and G. B. Northam, "Raman measurement of mixing and finite-rate chemistry in a supersonic hydrogen-air diffusion flame," *Combust. Flame*, vol. 99, pp. 157–173, 1994.
- [9] M. J. Cleary and A. Y. Klimenko, "A detailed quantitative analysis of sparse-Lagrangian FDF simulations in constant and variable density reacting jet flows," *Phys. Fluids*, vol. 23, no. 11, 2011.
- [10] A. W. Cook, "Artificial fluid properties for large-eddy simulation of compressible turbulent mixing," *Phys. Fluids*, vol. 19, pp. 1–9, 2007.
- [11] R. Borghi, "Turbulent combustion modelling," *Prog. Energy Combust. Sci.*, vol. 14, pp. 245–292, 1988.
- [12] F. A. Jaber, P. J. Colucci, S. James, P. Givi, and S. B. Pope, "Filtered mass density function for large-eddy simulation of turbulent reacting flows," *J. Fluid Mech.*, vol. 401, pp. 85–121, 1999.
- [13] S. Heinz, "On Fokker–Planck equations for turbulent reacting flows . Part 2 . Filter density function for large eddy simulation," *Flow Turbul. Combust.*, vol. 70, pp. 153–181, 2003.
- [14] C. A. Kennedy and M. H. Carpenter, "Several new numerical methods for compressible shear-layer simulations," *Appl. Numer. Math.*, vol. 14, pp. 397–433, 1994.
- [15] X. Tang and A. Xiao, "Efficient weak second-order stochastic Runge–Kutta methods for Itô stochastic differential equations," *BIT Numer. Math.*, vol. 57, no. 1, pp. 241–260, 2017.
- [16] C. A. Kennedy and A. Gruber, "Reduced aliasing formulations of the convective terms within the Navier–Stokes equations for a compressible fluid," *J. Comput. Phys.*, vol. 227, pp. 1676–1700, 2008.
- [17] D. V. Gaitonde and M. R. Visbal, "Pade-type higher-order boundary filters for the Navier–Stokes equations," *AIAA Journal*, vol. 38, no. 11, pp. 2103–2112, 2000.
- [18] C. W. Zhou, Y. Li, U. Burke *et al.*, "An experimental and chemical kinetic modeling study of 1,3-butadiene combustion," *Combust. Flame*, vol. 197, pp. 423–438, 2018.